

Calcination and sintering effects on the microstructure and dielectric properties of $\text{CaCu}_3\text{Ti}_4\text{O}_{12}$ ceramics

Lei Cao^a, Peng Liu^{a,*}, Jian-Ping Zhou^a, Ya-Juan Wang^a, Li-Na Su^a, Cheng Liu^a and Huai-Wu Zhang^b

^aCollege of Physics and Information Technology, Shaanxi Normal University, Xi'an 710062, China

^bThe Key Laboratory of Electronic Thin Film and Integrated Devices, University of Electronic Science and Technology of China, Chengdu 610054, China

$\text{CaCu}_3\text{Ti}_4\text{O}_{12}$ (CCTO) ceramics were fabricated by a conventional solid-state reaction at various calcination and sintering temperatures. Depending on the relative dielectric constant (ϵ_r) at 1 kHz, the specimens can be categorized into three types: type A ($\epsilon_r < 5 \times 10^4$), type B ($5 \times 10^4 < \epsilon_r < 10^5$) and type C ($\epsilon_r > 10^5$). The value of ϵ_r is closely related to the microstructure: type-A specimens show a morphology with large grains embedded in a small-grained matrix, type-B specimens present a network structure and type-C specimens display a core-shell structure. Different dielectric loss variation tendencies are observed in the type-A specimens, which can be well explained by impedance spectroscopy analysis and further confirmed by the EDX results. Also, the proper calcination and sintering temperature ranges needed to achieve good comprehensive properties are given.

Key words: Ceramics, Dielectric properties, Microstructure.

Introduction

With the size reduction of microelectronic devices, high-dielectric-constant materials have become increasingly important. Recently, much attention has been paid to $\text{CaCu}_3\text{Ti}_4\text{O}_{12}$ (CCTO) [1-3], which exhibits a high dielectric constant with good temperature stability.

Although considerable efforts have been aimed at understanding the origin of the dielectric behavior of CCTO, it still remains unclear. Nevertheless, it is now comparatively accepted that the high dielectric response is not an intrinsic effect but associated with some extrinsic effects [4-13], among which a grain boundary (internal) barrier layer capacitance (IBLC) effect is the most plausible [4-7]. For the grain boundary IBLC model, the relative dielectric constant ϵ_r is given by:

$$\epsilon_r \approx \epsilon_{GB} \frac{A}{t}, \quad (1)$$

where ϵ_{GB} represents the dielectric constant of the grain boundary phase, A is the average grain size and t is the average thickness of the grain boundaries. Apart from the IBLC model, the dielectric response of CCTO has also been suggested to be associated with a surface barrier layer [8-11] and internal domains [12-13]. So, more experimental evidence is required to understand the origin of the high dielectric response.

On the other hand, it is well known that fabricating CCTO ceramics for reproducibility and reliability in behavior is not easy, as they are sensitive to processing [14]. Two heating processes play important roles in controlling the final properties of the ceramics, i.e. calcination and sintering [15]. The effects of the sintering temperature [16-17], sintering times [4-6, 18-20] and both factors [10, 12, 21-23] have been intensively investigated, which indicate that raising the sintering temperature or extending the sintering time has a similar effect in enhancing ϵ_r of CCTO ceramics. However, little detailed research [24, 25] has been devoted to the influence of the calcination temperature on CCTO ceramics. It is essential to reveal its influence and find the proper processing parameters to obtain CCTO ceramics with optimized properties.

In the present study, $\text{CaCu}_3\text{Ti}_4\text{O}_{12}$ (CCTO) ceramics were fabricated by a conventional solid-state reaction method in wide calcination and sintering temperature ranges. Microstructural evolution and dielectric properties are highlighted as functions of the calcination and sintering temperatures. The proper calcination and sintering temperature ranges to achieve good comprehensive properties are determined.

Experimental

Stoichiometric amounts of high-purity CaCO_3 (99.99%), CuO (99.99%) and TiO_2 (99.99%) reagents were mixed and milled in ethanol using a planetary mill with zirconia media for 10 h. After drying, the mixture of the starting materials was calcined in air at 850 °C, 900 °C, 950 °C and 1000 °C for 6 h. The calcined powders were then uniaxially pressed into pellets which were 10 mm in diameter and 1.5 mm in thickness at a pressure of 170 MPa using PVA as binder. The

*Corresponding author:
Tel : +86-29-8530-3732
Fax: +86-29-8530-3823
E-mail: liupeng@snnu.edu.cn

pressed pellets were sintered in air at 1050 °C, 1080 °C, 1100 °C and 1120 °C for 10 h and then furnace-cooled to room temperature. The relative bulk densities of the sintered pellets measured by the Archimedes method were in the range of 94.0%-97.6%. For electrical characterization, the sintered pellets were polished to be with uniform parallel surfaces, coated with silver paste and fired at 500 °C for 30 minutes.

The crystalline structure was characterized by X-ray diffraction (XRD) carried on a D/max-2550/PC diffractometer (Rigaku, Japan) using Cu K α radiation (40 kV and 50 mA) in the 2θ range 20°-80° with a step of 0.02°. A scanning electron microscope (SEM, Quanta 200, Philips, Netherlands) equipped with energy-dispersive X-ray spectroscopy (EDX) was used to observe the microstructures and compositions. The dielectric property measurements were performed on an Agilent 4294A impedance analyzer in the frequency range from 40 Hz to 110 MHz.

Results and Discussion

Fig. 1(a) shows the XRD patterns of the calcined powders. The CCTO structure is formed with the presence of small amounts of TiO₂, CuO and CaTiO₃ phases at 850 °C. These minor phases gradually disappear with an increase in the calcination temperature. The crystal structures of the final specimens were also characterized by X-ray diffraction. All specimens are verified to be single phase CCTO. The XRD patterns of the 850 °C-calcined specimens (specimens sintered at various temperatures after calcined at 850 °C) are shown in Fig. 1(b) as a representation.

Fig. 2 demonstrates the relative dielectric constant for

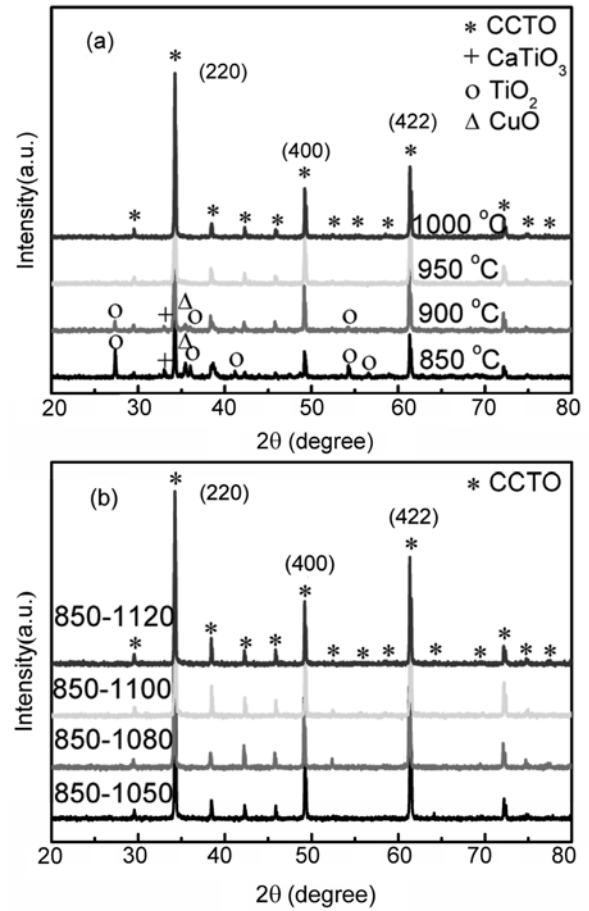


Fig. 1. XRD patterns of (a) calcined powders, (b) the specimens sintered at various temperatures after calcination at 850 °C.

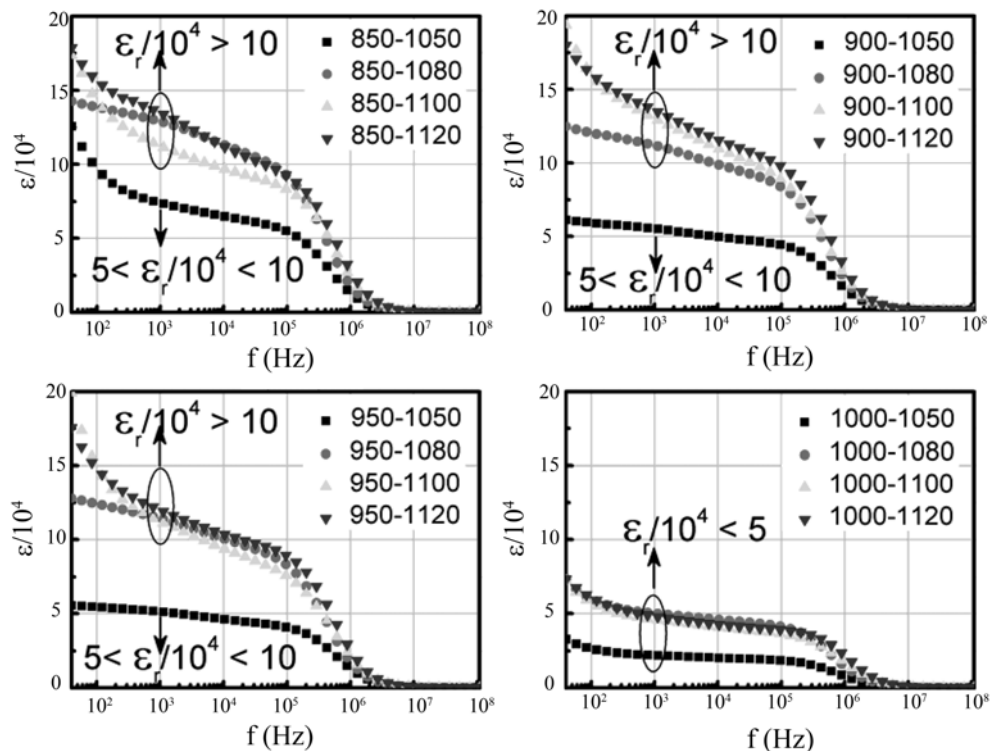


Fig. 2. Frequency dependence of the relative dielectric constant for the specimens obtained at various calcination and sintering temperatures.

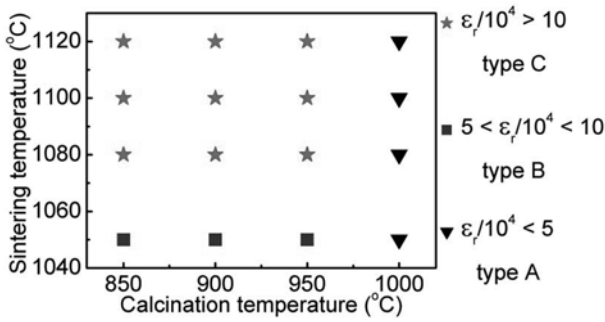


Fig. 3. The classification of the present specimens based on the value of the relative dielectric constant at 1 kHz.

various CCTO ceramic specimens measured at room temperature over the frequency range of 40 Hz-110 MHz. It is clear that ϵ_r changes significantly with the calcination and sintering temperatures. According to the value of ϵ_r

at 1 kHz, the specimens can be categorized into three types. The following terms will be used to narrate our results: type A (with $\epsilon_r < 5 \times 10^4$ at 1 kHz), type B (with $5 \times 10^4 < \epsilon_r < 10^5$ at 1 kHz) and type C (with $\epsilon_r > 10^5$ at 1 kHz), respectively. This classification is summarized in Fig. 3.

As exhibited in Fig. 4, the type-A specimen has a morphology with a few very large grains (around 50 μm) embedded in a small-grained matrix, which can be broadly described as these large grains floating in a “pool” of small grains. Also, the 1000-1050 specimen (the specimen sintered at 1050 $^\circ\text{C}$ after calcination at 1000 $^\circ\text{C}$) displays a much smaller average grain size compared with the other type-A specimens. According to Eq. (1), ϵ_r of the 1000-1050 specimen would be lower than that of the others, which is in accordance with the experimental result in Fig. 2.

Fig. 5 depicts the microstructures of the type-B specimens. Clearly, large grains (20-100 μm) isolated by some small

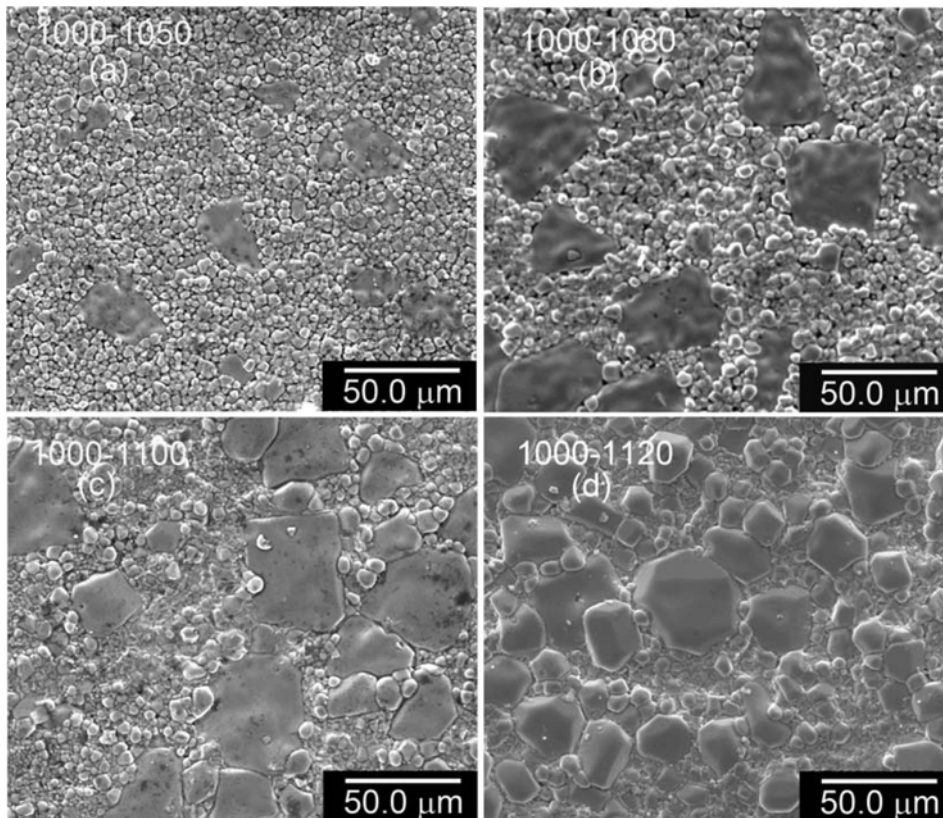


Fig. 4. SEM images of the type-A CCTO ceramics (in Fig. 3).

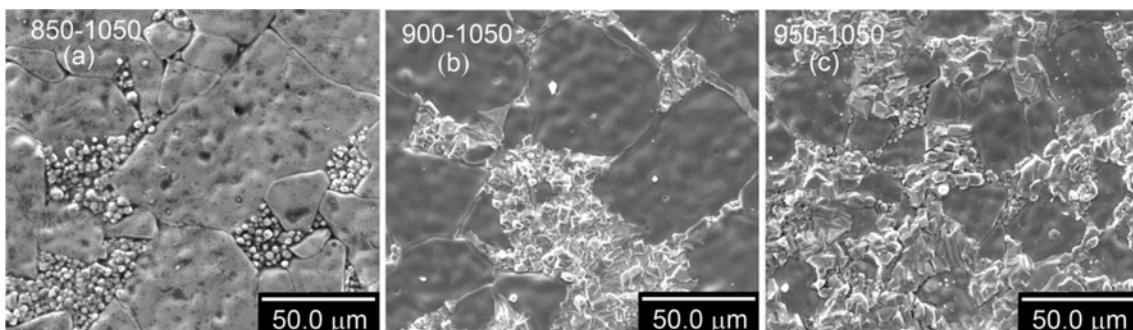


Fig. 5. SEM images of the type-B CCTO ceramics (in Fig. 3).

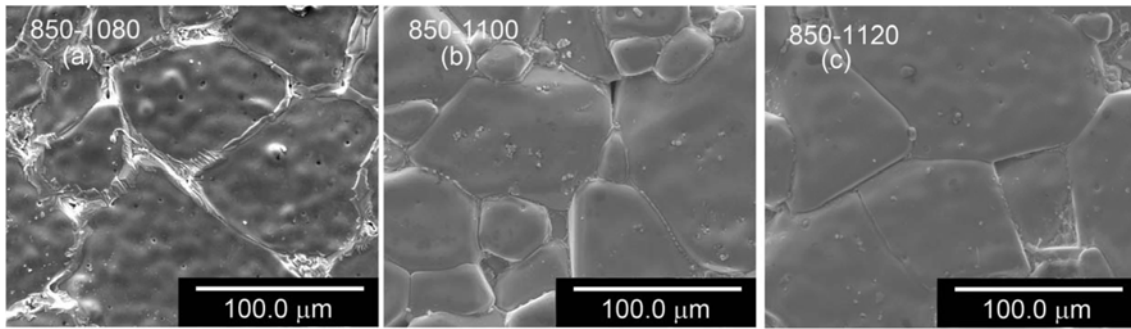


Fig. 6. SEM images of the representative specimens classified as type C (in Fig. 3)—the CCTO ceramics sintered at (a) 1080 °C, (b) 1100 °C and (c) 1120 °C after calcination at 850 °C.

grains (3–5 μm) impinge with each other to form a network structure. With an increase in the calcination temperature, from Fig. 5(a) to Fig. 5(c), the average grain size becomes smaller, leading to a decrease of ε_r (Fig. 2). A reduction of the average grain size can be interpreted by the effect of the CuO secondary phase contained in the calcined powders, since the content of CuO in the calcined powder gradually reduces as the calcination temperature is increased from 850 °C to 950 °C (shown in Fig. 1), and CuO is one of the best-known additives for promoting densification via liquid phase sintering [26–28].

Fig. 6 exhibits the surface morphologies of the type-C specimens. The fine grains surrounding the large grains in type-A and type-B specimens (Fig. 4 and Fig. 5) appear to have melted to become secondary phases at the grain boundaries. That is, a core-shell structure [29] is formed. It is also revealed that the thickness of the grain boundaries reduces with an increase of the sintering temperature from 1080 °C to 1100 °C and 1120 °C. Similar core-shell structures as well as morphological evolution with sintering temperature are observed in the 900 °C-calcined and the 950 °C-calcined specimens (not shown here).

A dissolution-precipitation sintering dynamic model [15] could be used to explain the morphological evolution of the specimens. For the type-B and type-C specimens, with an increase of the sintering temperature from 1050 °C to 1080 °C, small grains (Fig. 5) gradually melt and precipitate on the outer surfaces of the large grains to become the secondary grain boundary phases (Fig. 6). On further increasing the sintering temperature from 1080 °C to 1100 °C and 1120 °C, the secondary phases at grain boundaries continue to melt and are absorbed by the large grains. Hence, as shown in Fig. 6, a reduction occurs in the thickness of the grain boundaries. With the type-A specimens, the increase in the number of large grains by raising the sintering temperature can also be interpreted by the melting and precipitation behavior of the small grains.

On the basis of the observations above, some common characteristics exist in the microstructure of the same type of specimens. Regarding the same type specimens as a whole, the average grain size increases in the sequence of type A, type B and type C. Accordingly, the type with a larger average grain size exhibits a higher dielectric

constant (Fig. 3), which is consistent with Eq. (1). Thus, the microstructure-dependent dielectric response can be well explained by the IBLC model. What should be mentioned is that, as revealed in our previous study [30], unlike Nb-doped CCTO, the surface barrier layer capacitance (SBLC) effect only makes a weak contribution to ε_r of pure CCTO in the frequency range lower than 100 Hz. Thus, the SBLC effect could be ignored in the present study, in which ε_r at 1 kHz near room temperature is considered.

The variation tendencies of dielectric loss with frequency for CCTO ceramics are presented in Fig. 7. Obviously, at each sintering temperature, the type-A (1000 °C-calcined) specimens exhibit a different feature from the others: with the smallest $\tan\delta$ value at high frequencies ($f > 10^4$ Hz) and the largest $\tan\delta$ value at low frequencies. It has been indicated that the microstructure-dependent dielectric response of the present ceramics is related to the IBLC effect. Under the IBLC model, the loss tangent is approximately given by [31]:

$$\tan\delta = \frac{1}{\omega R_{\text{ins}} C_p} + \omega R_{\text{ins}} C_p \quad (2)$$

where R_{ins} represents the resistance of the insulating grain boundaries and R_{sc} is the resistance of the semiconducting grains. Their values can be obtained from the complex impedance plane plot: the diameter of the low frequency semicircle corresponds to R_{ins} , while the high frequency intercept on the Z' axis corresponds to R_{sc} .

Fig. 8 displays the complex impedance plane plot for the present specimens. The type-A (1000 °C-calcined) specimens show the smallest R_{ins} and the largest R_{sc} at each fixed sintering temperature. According to Eq. (2), $\tan\delta \approx 1/\omega R_{\text{ins}} C_p$ at low frequencies, the smallest R_{ins} together with the lowest C_p (Fig. 2) definitely results in the largest $\tan\delta$ at low frequencies, which agrees with the experimental result (Fig. 7). At high frequencies, $\tan\delta \approx \omega R_{\text{sc}} C_p$. Although R_{sc} of the type-A specimen shows a slight increase compared with others sintered at the same temperature (the inset of Fig. 8), the value of C_p drops markedly (Fig. 2), causing the reduction of dielectric loss at high frequencies.

It has been reported by Fang et al. that the excess Cu ions located at grain boundaries are directly related to the grain

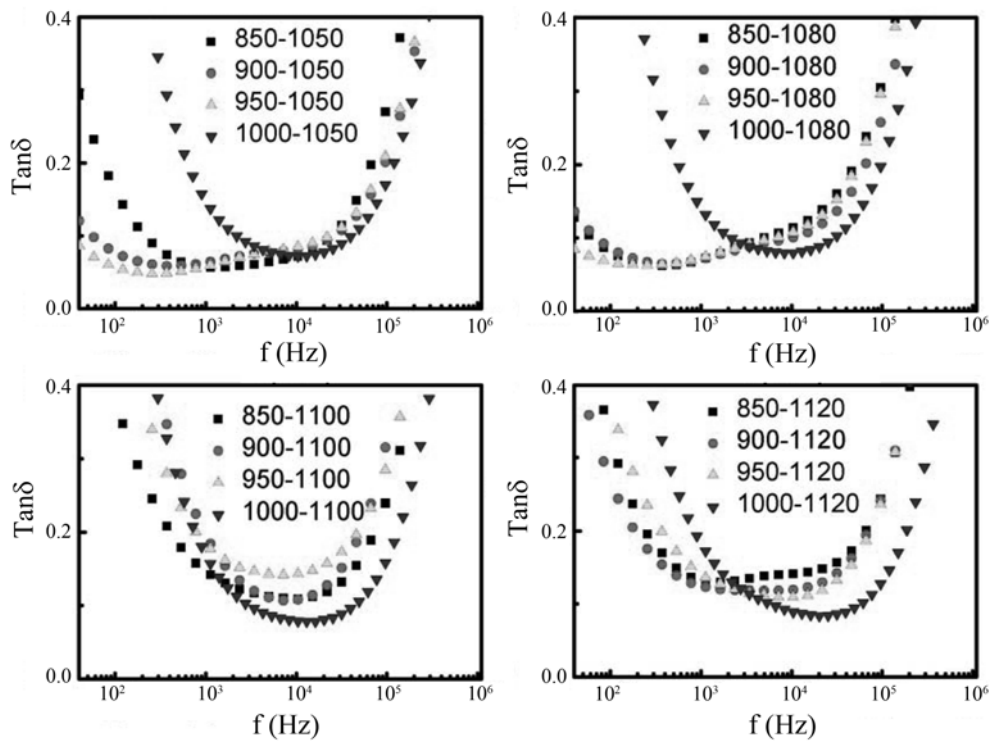


Fig. 7. Frequency dependence of loss tangent $\tan\delta$ at room temperature for the specimens obtained at various calcination and sintering temperatures.

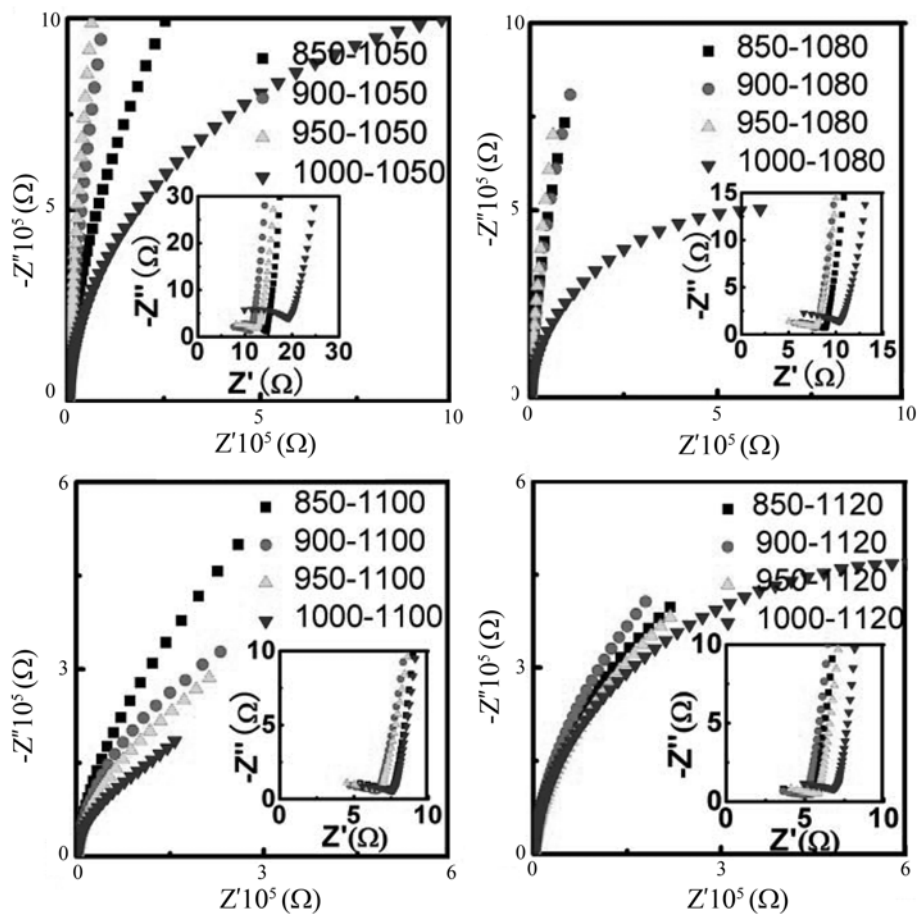


Fig. 8. Complex impedance plane plot for the specimens obtained at various calcination and sintering temperatures. The insets show expanded views of the high frequency data close to the origin.

boundary resistance [32]. To confirm that the type-A specimens do exhibit lower grain boundary resistance, EDX analyses were carried out in both the grains and the grain boundaries of CCTO ceramics prepared at various processing conditions. The results are shown in Table 1. The decimal part of the quantitative ratios has been approximated to simplify the format of the table. Table 1 reveals that the grain boundaries are clearly evidenced to be Cu rich, while the grains are nearly stoichiometric for all the specimens. This result is in accordance with the data provided by Fang and Mei [7] and Prakash and Varma [10]. It is also found that the concentration of the excess Cu ions at the grain boundaries is dependent on the processing. According to the degree of enrichment of Cu ions (atom %) at the grain boundaries, the specimens can be classified into two categories, as demonstrated in Fig. 9. Apparently, the type-A specimens show a reduction in the concentration of the excess Cu ions at the grain boundaries, which results in a lower space-charge potential [32] and induces the decrease in the grain boundary resistance (Fig. 8).

In considering the practical application of CCTO ceramics, specimens with good comprehensive properties should exhibit high ϵ_r as well as low $\tan\delta$. Also it has been revealed in Eq. (2) that a small R_{sc} and large R_{ins} are essential to keep $\tan\delta$ low over a wide frequency range. The type-A (1000 °C-calcined) specimens, with a low ϵ_r , large R_{sc} and small R_{ins} , do not meet the practical requirement of

CCTO ceramics. For the type-B and type-C specimens, at each fixed calcination temperature in the range of 850–950 °C, $\tan\delta$ varies a little as the sintering temperature is increased from 1050 °C to 1080 °C (Fig. 7), while ϵ_r shows a large magnitude enhancement (Fig. 2); on further raising the sintering temperature to 1000 °C and 1120 °C, there are no significant changes in ϵ_r (Fig. 2) but obvious increases in $\tan\delta$ (Fig. 7). Hence, the 1080 °C-sintered type-C CCTO ceramics exhibit better comprehensive properties than CCTO ceramics prepared with the other processing conditions.

Conclusions

The effects of calcination and sintering temperatures on the microstructure and dielectric properties of $\text{CaCu}_3\text{Ti}_4\text{O}_{12}$ ceramics were investigated. Based on the relative dielectric constant (ϵ_r) at 1 kHz, the ceramics can be divided into three types: type A ($\epsilon_r < 5 \times 10^4$), type B ($5 \times 10^4 < \epsilon_r < 10^5$) and type C ($\epsilon_r > 10^5$). Some common characteristics exist in the microstructure of each type: type-A specimens show a morphology with large grains embedded in a small-grained matrix, type-B specimens present a network structure and type-C specimens display a core-shell structure. Thus, the final ϵ_r is directly related to the microstructure. Different variation tendencies of the dielectric loss are observed in the type-A specimens, which can be well explained by the impedance spectroscopy analysis: the type-A specimens exhibit a higher grain resistance and lower grain boundary resistance compared with the others sintered at the same temperature. The lower grain boundary resistance of the type-A specimens is confirmed by a reduction of the excess Cu ions at the grain boundaries indicated in the EDX results. It is crucial to adequately control the processing parameters to obtain the desired dielectric properties and microstructures. High ϵ_r ($> 10^5$ at 1 kHz), low $\tan\delta$ with a core-shell microstructure can be achieved by sintering at 1080 °C after calcining in the temperature range of 850–950 °C.

Table 1. EDX results for the grains and grain boundaries of CCTO ceramics prepared at various calcination and sintering temperatures

Locations	Ca : Cu : Ti (Atom %)				
	Calcination temperature (°C)	Sintering temperature (°C)			
		1050	1080	1100	1120
Grain	850	6 : 18 : 25	7 : 20 : 29	6 : 18 : 24	6 : 18 : 25
	900	7 : 20 : 27	6 : 18 : 24	6 : 18 : 25	6 : 18 : 25
	950	6 : 18 : 26	6 : 18 : 26	7 : 21 : 27	6 : 18 : 24
	1000	6 : 18 : 22	6 : 18 : 24	6 : 17 : 22	6 : 18 : 25
Grain boundary	850	3 : 50 : 15	1 : 61 : 5	1 : 47 : 6	2 : 40 : 10
	900	1 : 56 : 6	1 : 62 : 5	4 : 46 : 17	6 : 42 : 30
	950	2 : 47 : 11	1 : 49 : 3	3 : 44 : 12	4 : 40 : 16
	1000	5 : 21 : 22	5 : 24 : 21	4 : 24 : 17	5 : 36 : 20

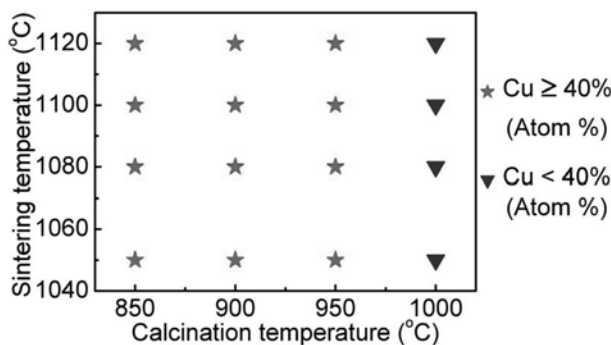


Fig. 9. The classification of the present specimens based on the degree of enrichment of Cu ions at the grain boundaries.

Acknowledgements

This study is supported by the National Natural Science Foundation of China (Grant No. 50872078 and 50772065), the National Basic Research Program of China (973) under Grant No. 2007CB310407.

References

1. C.C. Homes, T. Vogt, S.M. Shapiro, S. Wakimoto and A.P. Ramirez, *Science* 293 (2001) 673–676.
2. M.A. Subramanian, D. Li, N. Duan, B.A. Reisner and A.W. Sleight, *J. Solid State Chem.* 151 (2000) 323–325.
3. A.P. Ramirez, M.A. Subramanian, M. Gardel and G. Blumberg, D. Li, T. Vogt, S.M. Shapiro, *Solid State Commun.* 115 (2000) 217–220.
4. T.B. Adams, D.C. Sinclair and A.R. West, *J. Am. Ceram. Soc.* 89[10] (2006) 3129–3135.

5. G.Z. Zang, J.L. Zhang, P. Zheng, J.F. Wang and C.L. Wang, *J. Phys. D.* 38 (2005) 1824-1827
6. T.B. Adms, D.C. Sinclair and A.R. West, *Adv. Mater.* 14 (2002) 1321-1323.
7. T.T. Fang and L.T. Mei, *J. Am. Ceram. Soc.* 90[2] (2007) 638-640.
8. P. Lunkenheimer, V. Bobnar, A.V. Pronin, A.I. Ritus, A.A. Volkov and A. Loidl, *Phys. Rev. B* 66 (2002) 052105-1-4.
9. P. Lunkenheimer, R. Fichtl, S.G. Ebbinghaus and A. Loidl, *Phys. Rev. B* 70 (2004) 172102-1-4.
10. B.S. Prakash and K.B.R. Varma, *J. Phys. Chem. Solids* 68 (2007) 490-502.
11. C.C. Wang and L.W. Zhang, *Appl. Phys. Lett.* 88 (2006) 042906-1-3.
12. T.T. Fang and H.K. Shiau, *J. Am. Ceram. Soc.* 87[11] (2004) 2072-2079.
13. T.T. Fang, L.T. Mei and H.F. Ho, *Acta Mater.* 54 (2006) 2867-2875.
14. S.K. Jo and Y.H. Han, *J. Mater. Sci.* 20 (2009) 680-684.
15. Y.K. Li and Z.J. Zhou, in "Ceramics and Composites of Ceramic Materials" (Beijing Institute of Technology Press, 2007) p.69.
16. L. Ni, X.M. Chen, X.Q. Liu and R.Z. Hou, *Solid State Commun.* 139 (2006) 45-50.
17. S.F. Shao, J.L. Zhang, P. Zheng, W.L. Zhong and C.L. Wang, *J. Appl. Phys.* 99 (2006) 084106-1-11.
18. S. Aygün, X. Tan and J.P. Maria, *D. Cann, J. Electroceram.* 15 (2005) 203-208.
19. H.T. Yu, H.X. Liu, H. Hao, L.L. Guo, C.J. Jin, Z.Y. Yu and M.H. Cao, *Appl. Phys. Lett.* 91 (2007) 222911-1-3.
20. C.M. Wang, K.S. Kao, S.Y. Lin, Y.C. Chen and S.C. Weng, *J. Phys. Chem. Solids* 69 (2008) 608-610.
21. W.Q. Ni, X.H. Zheng and J.C. Yu, *J. Mater. Sci.* 42 (2007) 1037-1041.
22. B.S. Prakash and K.B.R. Varma, *J. Mater. Sci.* 42 (2007) 7467-7477.
23. J.J. Mohamed, S.D. Hutagalung, M.F. Ain, K. Deraman and Z.A. Ahmad, *Mater. Lett.* 61 (2007) 1835-1838.
24. B.A. Bender and M.J. Pan, *Mater. Sci. Eng. B* 117 (2005) 339-347.
25. M.J. Pan and B.A. Bender, *J. Am. Ceram. Soc.* 88[9] (2005) 2611-2614.
26. D.W. Kim, T.G. Kim and F.S. Hong, *Mater. Res. Bull.* 34 (1999) 771-781.
27. C.L. Huang and Y.C. Chen, *Mater. Res. Bull.* 37 (2002) 563-573.
28. C.L. Huang, M.H. Weng and C.C. Yu, *Ceram. Int.* 27 (2001) 343-350.
29. Q.R. Yin and B.H. Zhu, in "Microstructure, Property and Processing of Ceramics" (Metallurgical Industry Press, 2005) p.110.
30. P. Liu, Y. He, J.P. Zhou, C.H. Mu and H.W. Zhang, *Phys. Status Solidi A* 206 (2009) 562-566.
31. Y.Y. Yan, L. Jin, L.X. Feng and G.H. Cao, *Sci. Eng. B* 130 (2006) 146-150.
32. T.T. Fang, W.J. Lin and C.Y. Lin, *Phys. Rev. B* 76 (2007) 045115-1-8.